This is a repository copy of *Deformation-resilient embroidered near field communication antenna and energy harvesters for wearable applications*.

White Rose Research Online URL for this paper:
http://eprints.whiterose.ac.uk/154136/

Version: Published Version

FULL PAPER

ADVANCED
INTELLIGENT
SYSTEMS
Open Access

www.advintellsyst.com

Deformation-Resilient Embroidered Near Field Communication Antenna and Energy Harvesters for Wearable Applications

Lulu Xu, Zekun Liu, Xiao Chen, Rujie Sun, Zhirun Hu, Zijian Zheng, Terry Tao Ye,* and Yi Li*

E-Textiles have gained increasing momentum in wearable electronics recently. Conductive-yarn-based embroidered devices, with the advantages of being soft, deformable, breathable, and protective for the skin, play an important role in replacing many metallic counterparts. However, embroidered devices face many new challenges in their design methodology and fabrication processes, such as high resistivity and low Q value of the conductive yarns, as well as deformation of device geometries during wearing. Herein, a strain-free, deformation-resilient embroidery process for near field communication (NFC) coil antennas is introduced. Coil geometry can endure extreme deformation by stretching with up to 50% elongation, bending with curvature as small as 16 mm in radius, and can still maintain a relatively small variation in its inductance, resonant frequency, Q value, as well as its energy-harvesting capabilities. The embroidered coil antenna is used in an NFC-based battery-free body sensor system. Experiments demonstrate that the system can maintain a stable performance (voltage supply, temperature sensing, and reading range) under various deformation conditions.

1. Introduction

Near field communication (NFC) brings the convenience of wireless transmission and energy harvesting simultaneously within a short reading range. This advantage not only enables

its adoption in mobile payments and authentication but also finds its applications in body area networks (BANs), especially wearable medical BAN, where battery-less medical sensors are attached to human body or clothes, powered by the harvested energy, and sending sensing information back to the interrogators, all through a single NFC coil antenna.

For NFC-enabled wearable sensors, without the need of batteries, sensors can be implemented in a nonintrusive and aesthetic manner, i.e., attached to human skins or integrated into clothes. The wearable NFC sensors consist of a coil antenna, an NFC chip, and sensing devices (sometimes the sensing devices are built into the NFC chip), while the chips and sensing devices can be reduced into a tiny grain of silicon; it is the NFC coil antenna that cannot be easily minimized and concealed.

Current implementations of the flexible NFC sensor system are mainly focused on film-based devices. The approaches include utilizing graphene-based antennas on polymeric substrates,[1] etching copper film geometries on PET substrates,[2,3] as well as screen-printing and laminating of graphene ink on

L. Xu, Z. Liu
School of Materials
University of Manchester
Oxford Road, Manchester M13 9PL, UK

Dr. X. Chen
Department of Electronic and Electrical Engineering
The University of Sheffield
Sheffield S3 7HQ, UK

R. Sun
Bristol Composites Institute (ACCIS)
University of Bristol
Bristol BS8 1TR, UK

(iD) The ORCID identification number(s) for the author(s) of this article can be found under https://doi.org/10.1002/aisy.201900056.

Dr. Z. Hu
School of Electrical and Electronic Engineering
University of Manchester
Oxford Road, Manchester M13 9PL, UK

Dr. Z. Zheng
Institute of Textiles and Clothing
The Hong Kong Polytechnic University
Hong Kong, S.A.R., China

Dr. T. T. Ye
Department of Electrical and Electronic Engineering
Southern University of Science and Technology
Shenzhen, Guangdong, China
E-mail: yet@sustech.edu.cn

Dr. Y. Li
School of Materials
University of Manchester
Oxford Road, Manchester M13 9PL, UK
E-mail: henry.yili@manchester.ac.uk

**ADVANCED
SCIENCE NEWS**
www.advancedsciencenews.com

**ADVANCED
INTELLIGENT
SYSTEMS**
Open Access
www.advintellsyst.com

papers.[4] These devices are flexible enough for bending or twisting, but the substrates cannot endure large mechanical strain and elongation. Jeonghyun et al. first explored skin-like NFC antenna based on polyimide (PI) substrate, on which the device deforms along with the substrate. Its stretchability is subject to the covering materials and the substrate.[5,6] These NFC antennas can work under strains of up to 30% elongation.[6] PI substrates offer very high chemical and thermal stabilities as well as good biocompatibility.[7] However, these devices are not suitable for aesthetic wearing because they create a sealing and nonbreathable layer on the skin, which consequently blocks the heat and moisture transfer.

The ideal solution is to embroider NFC coil antennas directly onto fabrics. Textile-based antennas can best exploit the flexibility and porosity of fibers and fabrics, which are soft, deformable, breathable, and protective for the skin. Recently, many fibrous structures have been proposed, thanks to the advancement of nanotechnology that enables yarns with desired conductivity and mechanical properties.[8] With antennas being seamlessly embroidered into fabrics, NFC sensors can be concealed as part of the clothes. With much more convenience in user experience, the embroidered NFC system would find its expanded applications in clinical health monitoring and rehabilitation.

People are exploring different approaches in embroidering antennas with traditional embroidery processes,[9,10] in which conductive yarns are fabricated into various geometries. Recently, embroidered patch antennas,[11] thick transmission lines,[12] and RFID coils[13,14] have been reported. However, the structures were embroidered on nonstretchable fabrics that cannot contour with human body for BAN applications. Other approaches use multilayers of conductive yarns to reduce their resistance, but the devices flexibility are limited.

Compared with the previous approaches to embroider devices on nonstretchable fabrics, embroidering NFC coils on stretchable fabrics needs to resolve many new challenges, such as 1) Tradeoff between conductivity and stretchability: Conductive yarns have much higher resistivity as compared with metallic wires. To reduce the ohmic loss, much thicker yarns (with a larger diameter) have to be used, or the coil geometries have to use multiple embroidered layers/threads to increase the cross-section, while the multilayer structure is not easily stretchable, and the thick threads are also hard to be embroidered into a desired geometry. Table S1, Supporting Information, compares the resistivity and diameter of different conductive yarns. As we can see from the table, a thin stretchable geometry with a low resistivity seems to be a contradictory requirement. 2) Deformation during embroidering: In the embroidery process for coil-shaped geometries on stretchable fabrics, the stitches in different directions will have different strains on the fabrics. The unevenly distributed strain will deform the fabrics and cause bumps and folds. It is difficult to produce an accurate geometry of spiral line on stretchable fabrics. 3) Deformation by elongation: The strain will further deform the embroidered geometry under external elongation. The substrate fabrics, the upper threads, and the lower threads have different Young's moduli. When being stretched, the embroidered structure will have different elongations as compared with the substrate. This uneven deformation is even worse for conductive yarns with multi-layered structures,

which have much higher Young's modulus. An elongated embroidered coil on stretchable fabrics is shown in Figure S1, Supporting Information, a bump in the center can be easily seen. 4) Deformation during wearing: Embroidered antennas cannot avoid deformations when being worn on human body. Both elongation and bending can happen at different parts of the clothes.

The changes in geometry will result in changes of the electromagnetic properties of the NFC antenna, and it is difficult to provide a stable power supply for the NFC chips and sensors when the inductive coupling efficiency of the coil antenna is not stable. Coil antenna designers have to take the deformation factors into consideration and explore antenna designs that are insensitive to deformation.

To the best of our knowledge, no prior work was specifically focused on the materials, mechanics, designs, and embroidery processes for yarn-based NFC. In this article, we propose an embroidery process as well as deformation-resilient designs for spiral coil structures that have both low resistivity and high stretchability, namely, 1) A thread of high conducting yarn is fastened by zigzag stitches. This embroidery process can maintain a precise geometry during the embroidering process; it can also achieve an evenly distributed strain during elongation and stretching. 2) Moreover, the conventional Archimedes spiral coil has been revised by introducing a sine-wave modulation to ensure that the coil geometry deforms evenly on all directions with least strain.

These two mechanical improvements (zigzag fastening stitches and sin-wave modulation) will maintain good stretchability of fabrics and yarns and, in the meantime, allow the NFC coil to endure extreme stretching with up to 50% of elongation. Compared with a 30% uniaxial deformation in the conventional PI-based coils, the proposed textile-based coils at 50% uniaxial deformation exhibit much lower effective area variation. Thus, the proposed coils can maintain much more stable electromagnetic (EM) properties (such as the resonant frequency, S11, and Q value) under deformation and offer more stable energy for the load circuitry powered by the NFC antenna. At 50% uniaxial deformation, the inductance variations of the proposed coils are 10% for circular NFC antenna and 7% for square NFC antennas, respectively.

Experiments demonstrate that our proposed NFC designs can communicate and harvest energy from a smartphone with NFC function (Xiaomi Mix 2, in this case) and constantly provide direct current (DC) power to an NFC body sensor array with 24 temperature sensor-nodes. The temperature reading can be acquired by an APP built into the smartphone.

2. Theoretic Analysis of Energy Harvesting and Signal Coupling in NFC Systems

An NFC sensor system consists of an NFC chip with a coil antenna for both energy harvesting and wireless communication, driving a microcontroller and one or more sensor devices, as shown in Figure S2, Supporting Information. NFC tags and readers exchange information and energy through magnetic coupling. Both readers and tags use coiled antennas to form a coupled magnetic field. The energy transfer (energy harvesting) is achieved

through the induced current in the tag coil coupled in the magnetic field created by the reader coil, and the data transfer is achieved through the modulation of the EM field by modulating the impedance of the antenna input terminals at the tag and reader chip in a time-division multiplexing manner, as shown in Figure S2, Supporting Information.

The magnetic field strength generated by the reader coil depends on many factors, i.e., the current flowing in the reader coil, the geometry of the reader coil, as well as the distance between tag's coil and reader's coil. For a typical rectangular coil, the magnetic field strength can be expressed in Equation (1).

$$H \approx I_R N_R \frac{ab}{4\pi\sqrt{\frac{a^2}{4} + \frac{b}{2} + x^2}} \left(\frac{1}{\frac{a^2}{4} + x^2} + \frac{1}{\frac{b^2}{4} + x^2}\right) \quad (1)$$

where I_R is the electric current in the reader coil and N_R is the number of turns. x is the distance between the reader coil and tag coil, a and b are the length and width of the reader's rectangular coil, respectively.

The voltage (V_{ant}) generated on the terminals of the tag antenna is determined by the mutual coupling inductance M_{12} between the reader and the tag, which is

$$V_{ant} = M_{12} \frac{dI_R}{dt} \quad (2)$$

where the mutual coupling inductance between reader and tag antenna is expressed in Equation (3).

$$M_{12} = \mu_0 N_0 S_0 \frac{H}{I_R} \quad (3)$$

Assuming a continuous cosine wave current is running in the reader coil, the induced voltage on the tag's coil terminals can be determined by Equation (4).

$$V_{ant} = j\omega\mu_0 H N_0 S_0 \quad (4)$$

where N_0 and S_0 are the number of turns and the effective area of the tag's coil, respectively. ω is the angular frequency of the electrical signal. μ_0 is the free space permeability.

Under a stable magnetic field created by the reader, to maintain a stable harvested energy (as determined by the terminal voltage of the tag coil) as well as a stable NFC signal strength, the effective area of the tag's coil S_0 has to be stable under different deformations and elongations.

3. Results and Discussions

3.1. Embroidery Process for the Stretchable Coil Antenna

Traditional embroidery techniques use inter-locked stitches to form the geometry, which not only imposes high tensions on the substrate fabric, the structure is also hard to be stretched during wearing. The embroidered geometry is not suitable for BAN applications. To solve this problem and achieve both high conductivity and stretchability, we use a single high conducting thread to form the coil geometry and use zigzag stitches to fasten the conducting thread in place, as shown in **Figure 1**a.

The high conducting thread is made of copper fibers, twisted and covered with highly stretchable nylon yarns (TIBTECH Innovations, Figure 1b), which exhibits a 10% yield and 50% fracture strains (Figure S3, Supporting Information). The copper-based conducting thread has a diameter of 350 μm and cannot be used as stitches; instead, the thread is laid on top of the substrate fabrics and fastened by the zigzag stitches. The width of the zigzag stitches ($d = 450$ μm) is slightly larger than the diameter of the conductive thread ($d = 350$ μm), so that the conducting thread can move along the stitches when the substrate fabrics is elongated or stretched.

Furthermore, because the conducting thread is on top of the substrate, the substrate fabric serves as an insulating layer between the NFC coil and the human body. Therefore, this method can also reduce the detuning effect on the coil antenna from the human body.

3.2. Deformation-Insensitive Coil Antenna Design

To further reduce the strains on the substrate during deformation, we revise the conventional coil spiral with a sine-wave modulation. Magnified view of regions of the coil is shown in Figure 1c, in which the conductive threads are on top of the substrate and fastened by the zigzag nonconductive yarns. Figure 1c, d shows the structure of the yarn-based circular ($d = 62$ mm) and square ($d = 42.8$ mm) coil antennas. The detailed design specifications are shown in Figure S4, Supporting Information.

Experiments show that this design can ensure that the coil geometry stretches evenly on all directions during elongation, avoiding bumps between the embroidery regions or inside the coil regions as compared with convention spiral coil in **Figure 2**a.
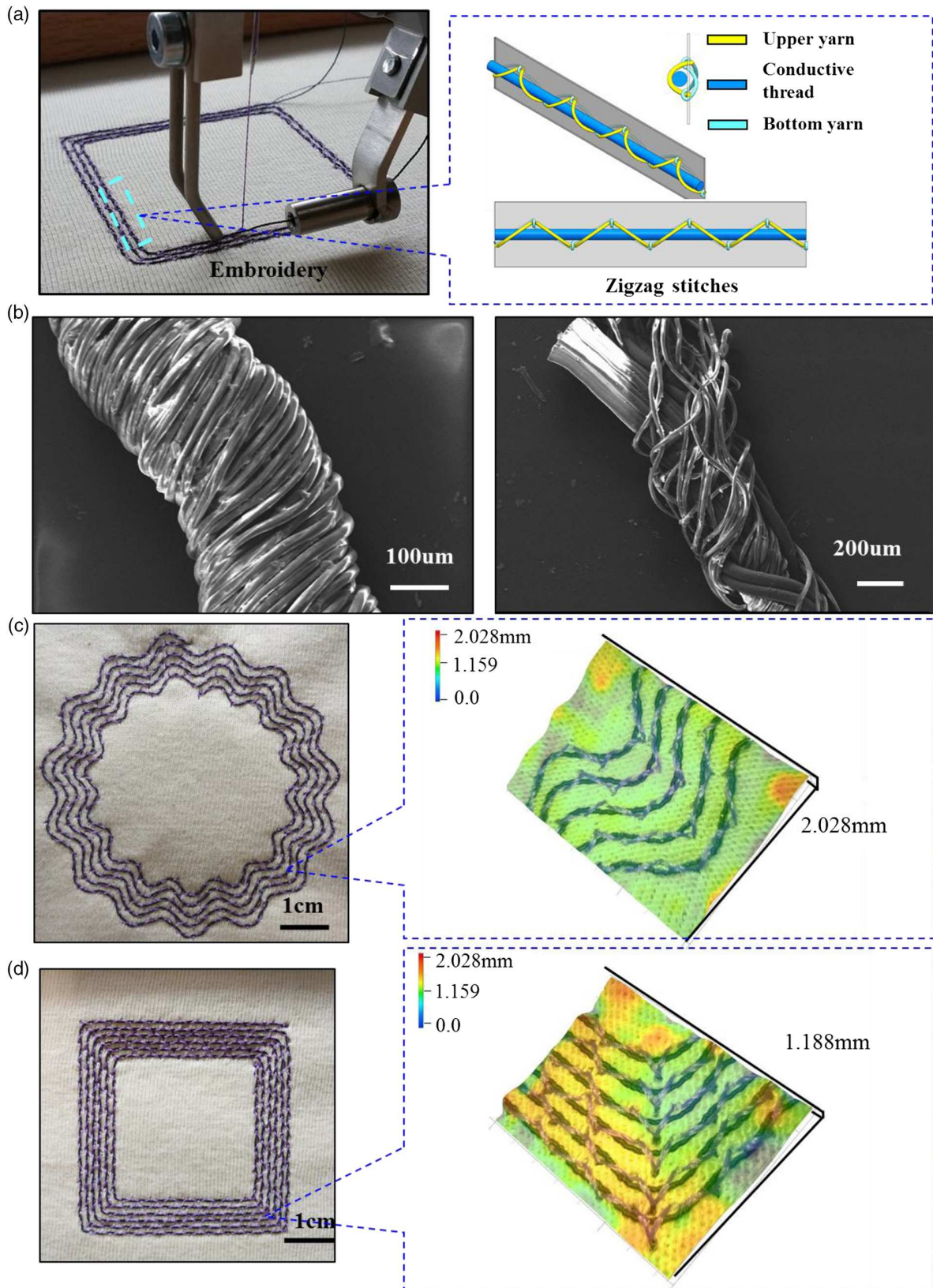
To ensure stable energy harvested from the NFC coil under deformation, the coil's magnetic flux area should be insensitive to the geometrical variations, particularly, the area S_0, as enclosed by the coil should keep stable. Poisson ratio is used in our analysis to measure the stability of the enclosed area S_0. Poisson value close to 1.0 means the coil is elongated in the stretching direction, but narrowed in the perpendicular direction equally; thus, the enclosed area is unchanged.

The substrate fabric is knitted by an interlock jersey structure, with its Poisson ratio = 0.6. After embroidering with the zigzag stitch, its Poisson ratio is increased to almost 1.0 (Figure S5 and S6, Supporting Information). The coil's structural variations can also be seen in Figure 2b,c; when being stretched, the spacing between the thread in the stretching direction increases, while the spacing between the threads in the perpendicular direction narrows. The spacing changes in these two directions cancel out each other, and the enclosed area S_0 as well as the inductivity of the coil will be almost stable.

3.3. Strain Analysis under Deformations

The fabrics worn on the human body may sometimes be stretched with up to 20% of elongation, depending on the types of clothes and its position on the body.[15] Figure 2 shows circular and square coils under uniaxial deformations, with 10%, 20%, 30%, 40% up to 50% elongation, along with the illustration of

ADVANCED
SCIENCE NEWS

www.advancedsciencenews.com

ADVANCED
INTELLIGENT
SYSTEMS
Open Access

www.advintellsyst.com

Figure 1. Proposed embroidery processes of the NFC coils a) Conductive threads fastened by the zigzag stitches. b) SEM images of the conducting copper yarns twisted and covered with nylon yarns. c,d) Images of embroidered conductive yarn-based circular ($d = 62$ mm) and square ($d = 42.8$ mm) coil antennas.
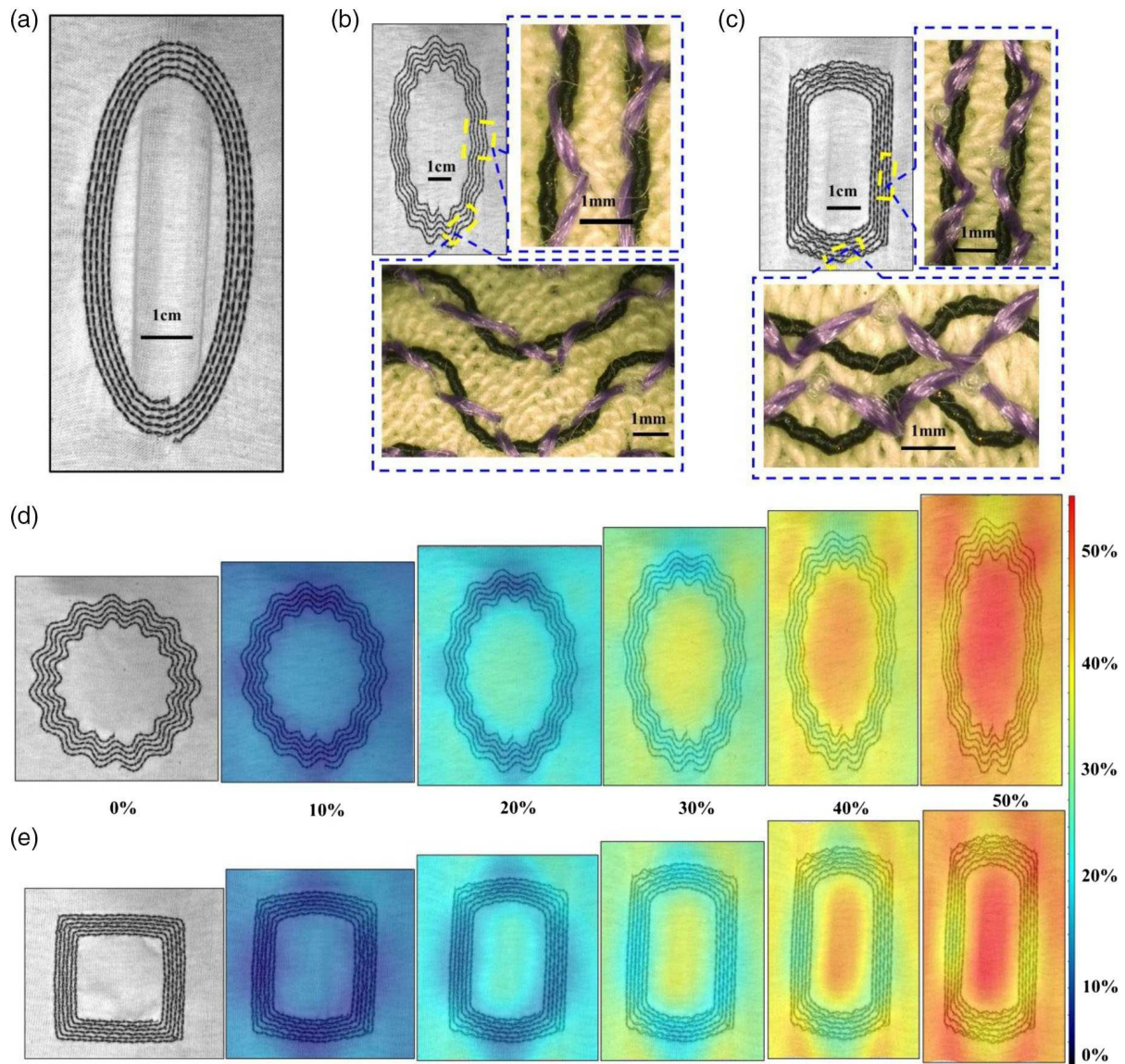
Figure 2. Pictures, optical microscope images, and von Mises distributions of circular and square coils under uniaxial deformations. a) Bumps/folds on conventional circular coil under uniaxial deformation up to 30% of elongation. b) Picture of a circular sine-wave coil under uniaxial deformation and corresponding optical microscope images of its structure variations in stretching and perpendicular directions. c) Picture of a square coil under uniaxial deformation and corresponding optical microscope images of its structural variations in stretching and perpendicular directions. d,e) Maximum von Mises strains distributions on circular and square coils with 10%, 20%, 30%, 40% up to 50% elongation, respectively.

von Mises strain distributions. The instruments used for the measurements are shown in Figure S7, Supporting Information.

Figure 2d,e illustrates the coils under these different elongations. The circular and the square coils are deformed into an elliptical and rectangle shape, respectively, in which the amplitude of the sine modulation along the elongation direction decreases and tends to straighten up, while the amplitude of the sine modulation on the other (perpendicular) direction increases along with the spacing in between the threads.

The von Mises strain illustrations further demonstrate the strain distribution, namely, 1) When coils are stretched with 10%, 20%, and 30% uniaxial elongation, the strains are distributed evenly across the entire substrate, as shown with the same color inside the coil region, the embroidery region, as well as the region outside of the coil. 2) When the deformation reaches 40% elongation, the stress inside the coil region is built up, while the embroidery region under the coil still maintains a relatively uniformed stress. 3) When deformation increases to 50% of uniaxial elongation, the strains are built up across the entire substrate. From the color map, we can observe that the strains on the corners of the coils are about 5% higher than those in the other regions. However, this 5% difference in strain normally cannot create noticeable bumps or folds on the substrates, and the entire fabric will still be smooth in appearance.

**ADVANCED
SCIENCE NEWS**

www.advancedsciencenews.com

**ADVANCED
INTELLIGENT
SYSTEMS**
Open Access

www.advintellsyst.com

These results show that both circular and square coils fabricated with our proposed embroidered process maintain high stretchability under extreme elongation. In fact, these coils can also stabilize their magnetic coupling area S_0 under extreme elongation as well.

We measured the changes of the effective area as the ratio (ρ) of the varied area to the original area, where

$$\rho = \frac{\Delta S}{S_0} \tag{5}$$

The value of ρ is estimated by calculating the area in the digital images (through Photoshop CC2015, Adobe) under different elongations, the results are shown in Table S2, Supporting information. We can see that the areas of our designs remain stable under different elongations, i.e., when the elongation reaches 50%, the area S_0 is increased by 8.29% and 4.11% for circular and square coils, respectively. Compared with the PI-based coils, these area variations are much smaller. As reported in the study by Kim et al.,[6] even under 30% elongation, the area changes are 10.5% and 16.4% for square and circular coils, respectively.

The experiments demonstrate that our proposed NFC coils are more resilient to extreme deformations. The coils will provide a stable harvested energy source and signal strength for NFC applications.

3.4. Electromagnetic Properties of Proposed Embroidered Coils

The embroidered coils serve both as antennas as well as energy harvesters in NFC applications. We use the NFC chip (NXP NTAG NT3H2111) to drive the coils. The chip has an input capacitance of 50 pF, and therefore, the coils are conjugate-matched with an equivalent input inductance of 2.75 μH that can achieve a resonant frequency of 13.56 MHz ($f = 1/2\pi\sqrt{LC}$), as required by the NFC operation.

The coil's EM properties, including the S11 parameter, inductance (L) and Q value, are measured at different elongations, and the results are illustrated in **Figure 3**. Measurements are performed on a Vector Network Analyzer (Keysight AFN9918A-M2) with a frequency span from 1 to 20 MHz.

From the results, we can see that the changes in inductance under different elongations align well with the changes in the coil's coupling area, as shown in Table S2, Supporting information. The relationship is straightforward to notice. 1) Under no strains (no elongation), the circular and square coils exhibit an inductance of 2.810 and 2.648 μH and a resistance (R) of 6.2 and 5.2 Ω, respectively. 2) Under 50% elongation, the inductance gradually rises to 3.106 and 2.835 μH (Figure 3a,b) with a change ratio ($\Delta L/L$) of 10% and 7% that agrees with the area changes of 8.29% and 4.11% for circular and square NFC antennas, respectively. 3) The resonant frequency at no elongation is 13.89 and 13.88 MHz, for the circular and square coils, respectively. Under 50% of elongation, the resonant frequency moves to 13.36 and 13.13 MHz, respectively (Figure 3b). 4) The Q value (Figure 3c) increases slightly with elongation. Specifically, under the elongation of 50%, the Q value rises from ≈39 to ≈44 for circular coil and from ≈45 to ≈48 for square coils, respectively. The increases in Q values agree with the increases in coupling areas, S_0, which, under 50% elongation, increase to 8.29% and 4.11% for circular and square coils, respectively.

The surface curvature of the human body will create stress and elongations on the embroidered coils. To estimate the impacts of the curvatures at different parts of the human body, such as back, chest, forearm, and wrist, the coils are bent at different curvature radii ranging from 81, 54, 36, 24 to 16 mm, respectively. The coil's effective area decreases with the increased bending curvature, leading to a decrease in the inductance, as well as an increase in the resonant frequency consequently.

As shown in **Figure 4**, even when the coils are extremely bent with a curvature radius of 16 mm, the inductance decreases to 2.683 and 2.557 μH (from 2.810 and 2.648 μH), with variations of 5.0% and 4.8%; the resonant frequency increases to 14.12 and 14.30 MHz (from 13.89 and 13.88 MHz); Q value rises to ≈44 and ≈49 (from 39 and 45) for circular and square coils, respectively.

The restorability and repeatability of the embroidered coils under repeated stress and elongation have also been tested. As shown in **Figure 5**a, the circular sine-wave antenna is stretched up to 30% elongation in 20 cycles; its inductance varies between its lower values (around 2.70 μH) and upper values (around 2.85 μH) during the repeated cycles; the lower values and upper values remain stable within 4% of variations.

For being used as wearable devices, human body's effect on the coils is also tested, as shown in Figure 5b,c. The inductance and the resonant frequency of the coil are measured in two cases, with and without attaching to the human body (in our test, it is the arm). As seen from the figures, human body has really insignificant effects on the inductance and resonant frequency of the embroidered coils. NFC coils use magnetic coupling to communicate with the interrogators, human body, which consists of mostly water, has less effects on the magnetic field.

Also note that the Q values of our embroidered coils are comparable with those of the commercial coils. Commercial metallic coils have Q values typically between 10 and 30.[6] This result is also much better than film-based or other embroidery coils shown in Figure S8, Supporting information.[1,9,13]

These experimental results demonstrate that our proposed embroidered NFC coils are resilient to extreme deformation of stretching and bending. They are ideal to be used for wearable applications where deformation from human body is unavoidable.

3.5. NFC-Based Battery-Free Body-Sensing System

We have built a complete energy-harvesting NFC wearable body sensor system (for breast cancer monitoring) using the proposed embroidered NFC coil antenna, together with the NXP NFC-tag (NTAG) NFC chip (NT3H2111), and an microcontroller (MCU) chip to drive a sensor array of 24 temperature sensors, as shown in **Figure 6**a,b. The circular sine-wave antenna is used in this case.

The MCU is a 16-bit RISC CPU, powered by the energy harvested from the NTAG chip through the V_{out} terminal. The data and control signal are connected through an I²C interface with the NTAG. The sensor node is connected to the MCU through another I²C interface, also powered by the DC supply from the harvested energy of the NFC chip. The device is embroidered onto a bra to form the NFC-based breast cancer–monitoring system. The schematic of the temperature monitoring bra is shown in Figure 6a,b, in which the sensors are homogeneously distributed on the hemisphere area of breasts.
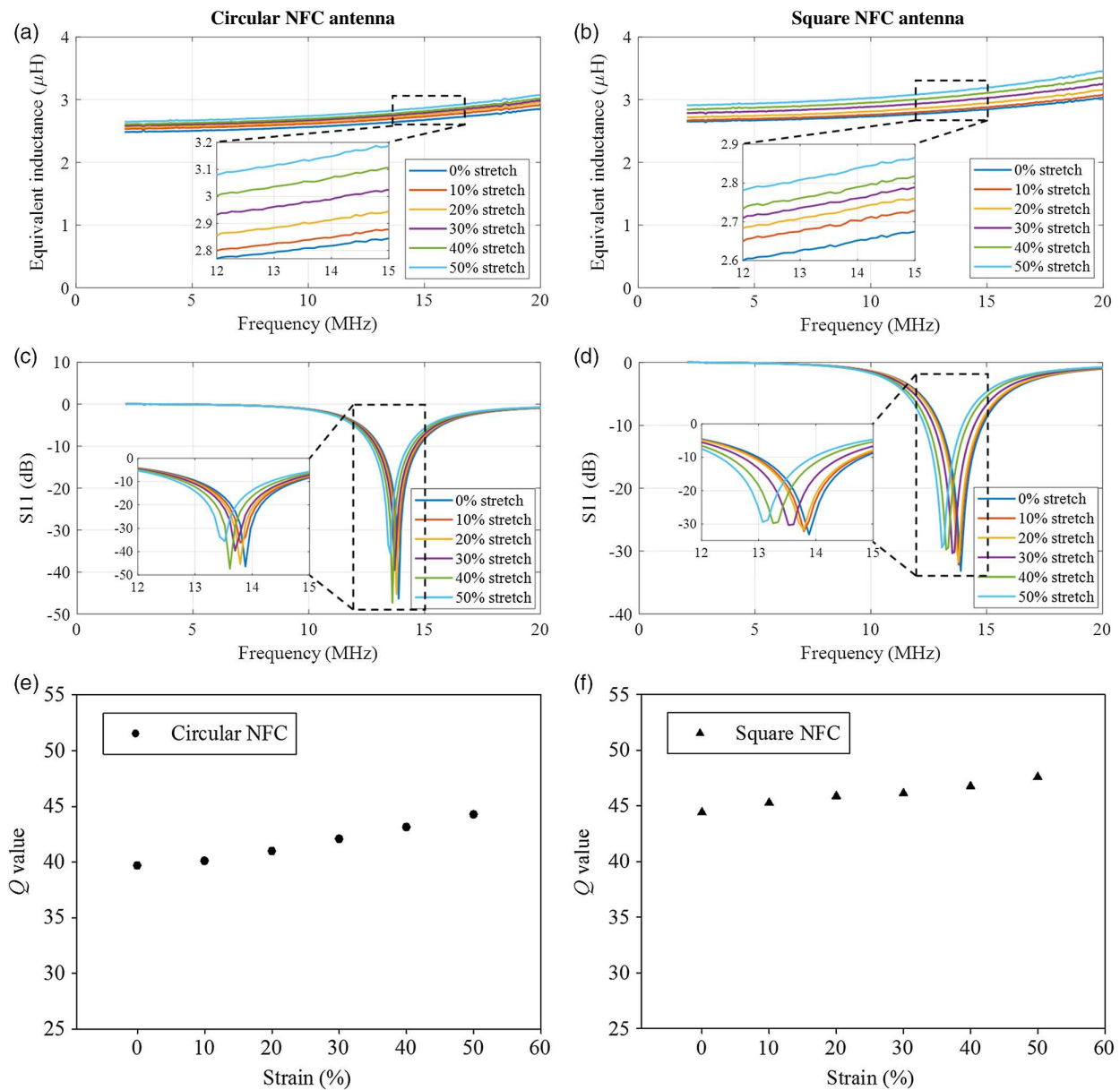
Figure 3. Experimental results of the coil's EM properties under uniaxial deformation with 10%, 20%, 30%, 40% up to 50% elongation. a,b) Circular and square coils inductance. c,d) Circular and square coils S11 parameters with respect to resonant frequencies. e,f) Circular and square coils Q values.

Thermography is an indicator of many physiological states of the human. The skin temperature can reflect the tissue state and can be used for early detection of tumor malignancies. The NFC-based bra-sensing system is to be used for the prognosis of breast cancer, because the increased metabolism and blood perfusion around the tumor will rise the surface temperature of the skin.[16] Traditional thermography is acquired through IR imaging, which is not accurate enough and has to be conducted in a strict laboratory environment. Using the NFC-sensing system, temperature data can be collected wirelessly and continuously in a noninvasive manner, which makes the monitoring process more conformable.

The energy harvested from the coil antenna is illustrated in Figure 6c, represented as the alternating current (AC) voltage

(V_{ant}) harvested from the NFC reader (TRF7970A), and the DC voltage (V_{out}), rectified from V_{ant} to power up the MCU and sensor array. Load resistances are connected to the DC source as loads. When the tag-to-reader distance is around 1 cm, for the load resistance larger than 1000 Ω; the antenna terminal voltage V_{ant} can stay above 3.2 V and the rectified DC V_{out} stays above 2.5 V. This indicates that the harvested DC power can generate at least 2.5 mA under 2.5 V, which is equivalent to 6.25 mW. The complete sensor system (including the MCU, the sensor array, and the switches) has a total power consumption of 870 μW. The NFC energy harvester can provide more than enough energy for the sensor system.

The reading distance between the NFC reader and tag antenna is determined by the minimum magnetic field strength H_{min} that
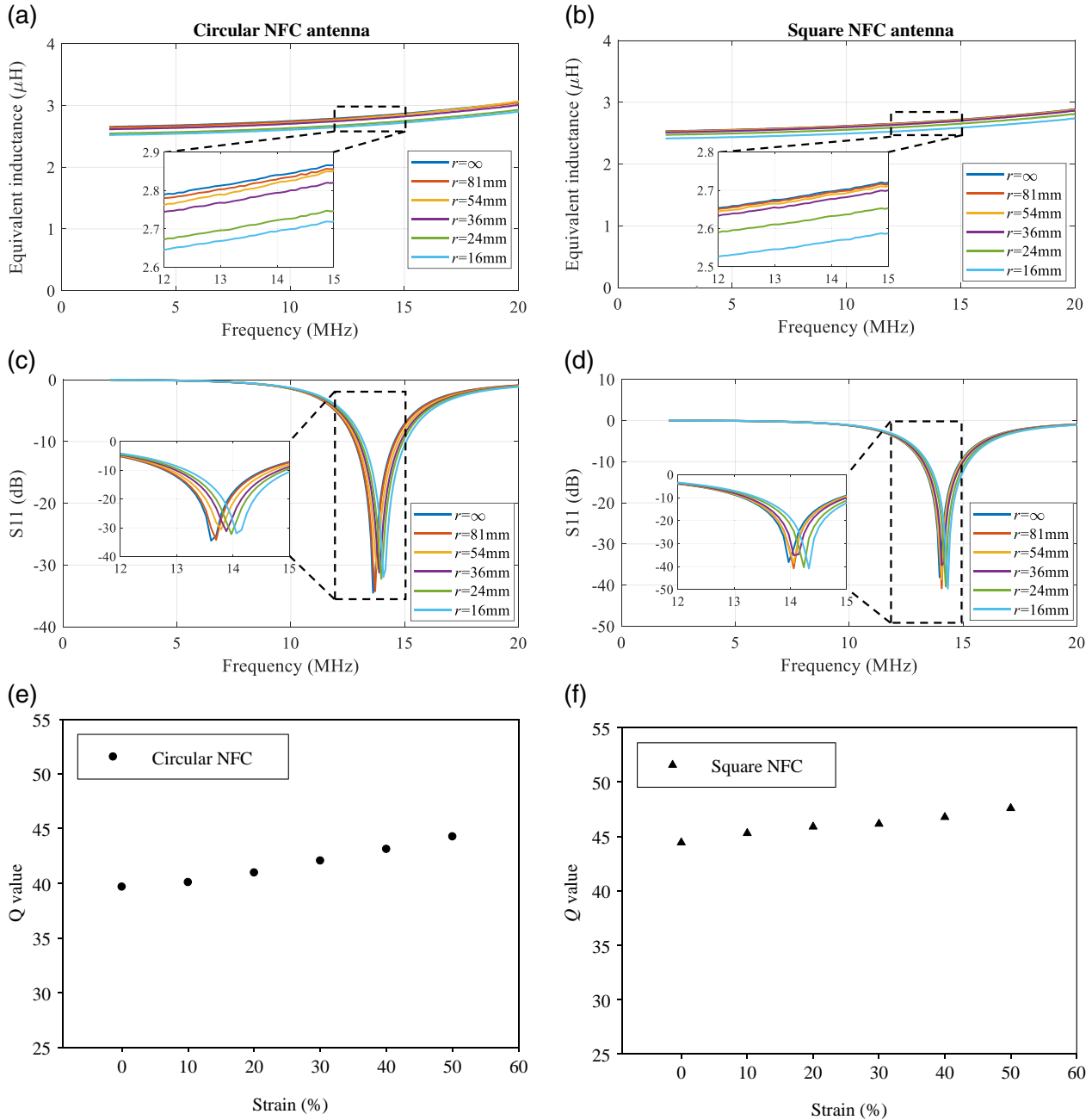
Figure 4. Experimental results of the coil's EM properties under bending curvature of 81, 54, 36, 24, and 16 mm. a,b) Circular and square coils inductance. c,d) Circular and square coils S11 parameters with respect to resonant frequencies. e,f) Circular and square coils Q values.

can create the minimum antenna terminal voltage V_{ant} for rectification. The relationship between H_{min} and V_{ant} can be expressed in Equation (6).[17]

$$H_{min} \approx \frac{V_{ant}}{2\pi f \mu_0 S_0 N_0 Q} \tag{6}$$

when the NFC chip is also driving an external load with power consumption of P_{load}, the threshold H_{min} will be increased, as shown in Equation (7).

$$H_{min} \approx \frac{1}{\mu_0 S_0 N_0 V_{ant}} \sqrt{\left(2 P_{load} L + \frac{V_{ant}^2}{2\pi f Q}\right)^2 + \left(\frac{2 P_{load} L}{Q}\right)^2} \tag{7}$$

when load power (P_{load}) increases, the threshold (H_{min}) rises, and therefore the reading distance has to be decreased to harvest enough energy from the reader antenna.

We tested the relationship between the load of NTAG chip and the maximum reading range. As shown in Figure 6d, as the load resistance decreases (more load), the maximum distance (x) will
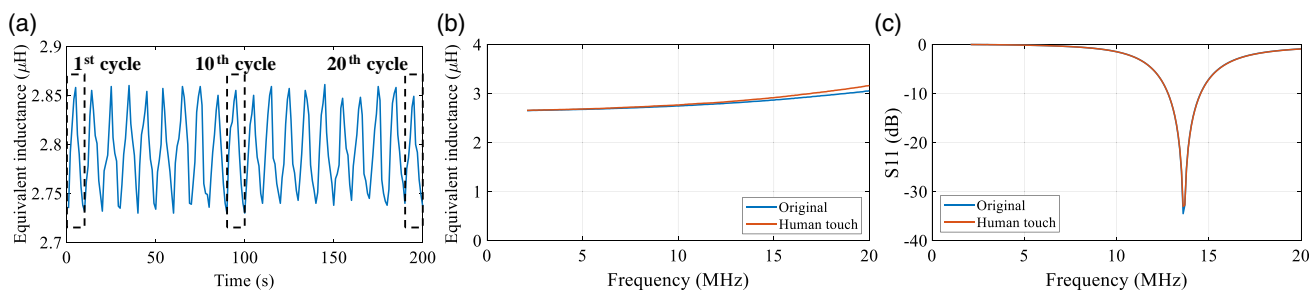
Figure 5. Experimental results of the coil's EM properties under dynamic movements and human body. a) Circular coils inductance under 20 cycles stretching. b) Circular coil inductance variation by human wearing. c) Circular coil resonant frequency variation by human wearing.

decrease accordingly, from 7.5 to 2.3 cm, while the antenna terminal voltage V_{ant} is stabilized at around 2.3 V.

An Android-based APP is created to extract the tag information as well as read the temperature from the sensor array, shown in Figure 6e. For this multiplexed operation, communication and power delivery occurred in 24 sensors in a time-sequential manner continuously, such that all 24 sensors can be read within 7 s. After a simple calibration, the reading temperatures are steady and match well with the thermal stimulus from a stream of heated air. As shown in Figure 6f,
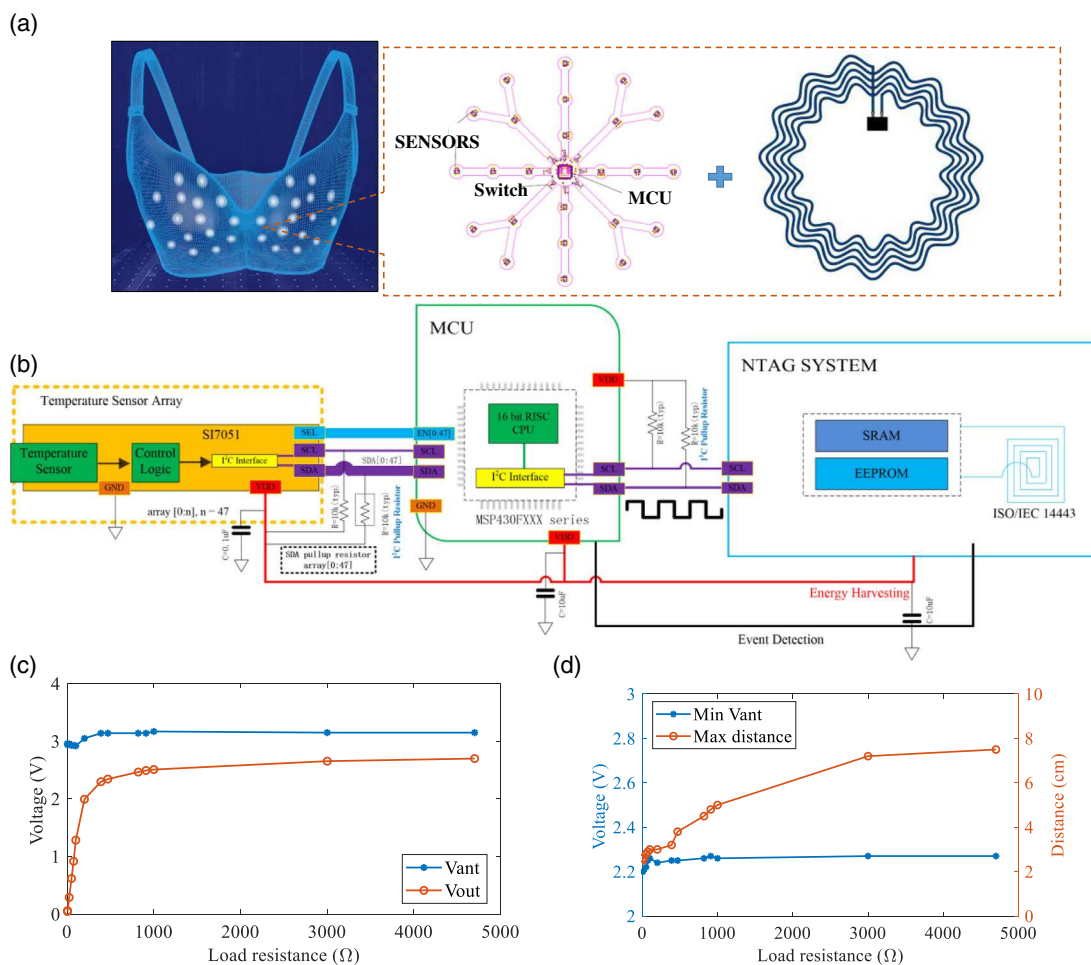
Figure 6. NFC-based battery-free body sensing system. a) Exploded-view and schematic illustration of the temperature monitoring bra. b) Circuitry schematic of the NFC-powered temperature-sensing system. c) Harvested voltage at the NFC antenna terminals. d) The maximum reading distance (right) and the rectified DC voltage (left) under different loads. e) Android-based APP for NFC communication and sensing temperature acquisition. f) The fluctuation of the sensing temperature at different controlled temperatures of 33, 35, 37, 39 and 41 °C, respectively. g) The Newton thermal manikin system used for temperature-sensing experiments. h,i) The acquired temperatures of right-side and left-side bra on the manikin, with temperature set from 35 to 39 °C.
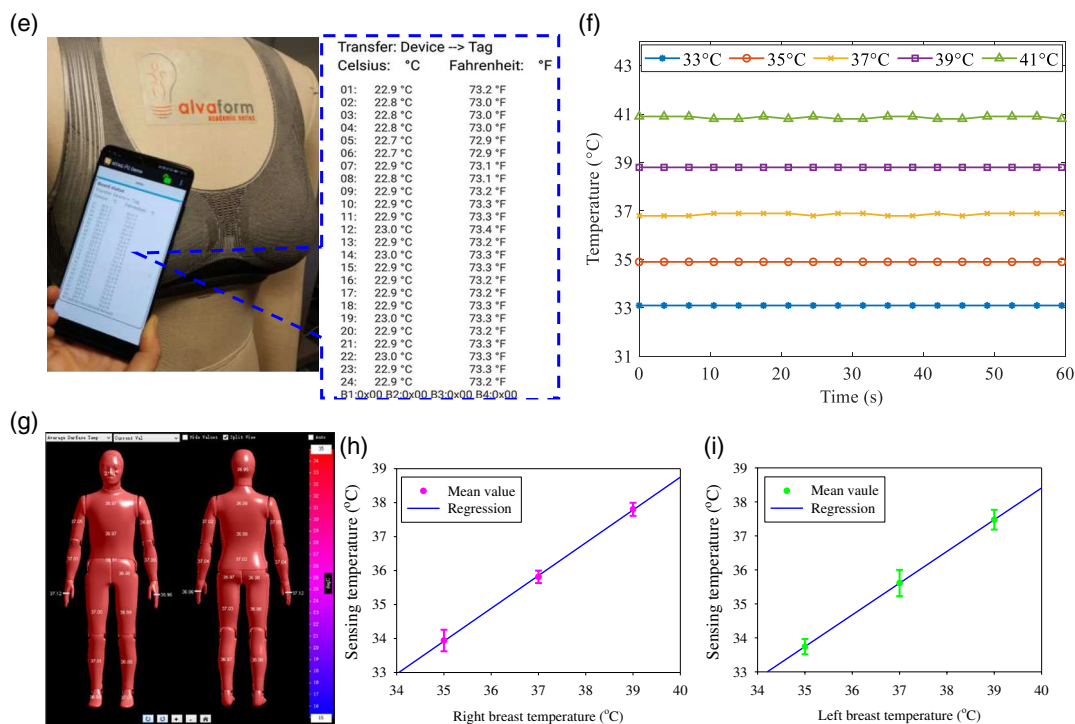
Figure 6. Continued

the stream of heated air is controlled at 33, 35, 37, 39, and 41 °C, respectively, and the differences of the sensed temperature are less than 0.1 °C.

To demonstrate the wearing conditions and to investigate the utility of wireless-sensing system for the detection of breast temperature, we performed studies with a Newton thermal manikin system in an ambient laboratory environment (Table S3, Supporting Information). The manikin body temperature is controlled from 35 to 39 °C; the sensing temperature of right and left breast from the NFC system is increasing linearly in this range, shown in Figure 6h,i respectively. The results demonstrate that the NFC-based bra exhibits stable, reliable performance in measuring body temperature and has the potential to be used as a breast temperature monitoring system for the early prognosis of breast cancer.

4. Conclusion

In this article, we have presented a deformation-insensitive embroidered NFC antenna design technique, which includes a strain-free embroidering process for high conductive coil structure and a few elongation-resilient coil designs. We used this technique to build a complete NFC-based energy-harvesting body sensor network and demonstrate that the NFC chip together with the embroidered coil antenna can generate stable harvested energy under extreme deformation. The complete sensor system can be stably powered by the harvested energy and can be used as a wireless battery-less body temperature–monitoring system.

5. Experimental Section

Fabrication of the Coils: The coils were fabricated by a commercial embroidery machine (JCZA 0109-550 (700), ZSK Stickmaschinen GmbH). In the first step, stitches were designed in the embroidery software (EPC, ZSK Stickmaschinen GmbH, embroidery design software). Then, the spiral-lines were punched with zigzag stitches with a thread length of 1 mm and width of 0.45 mm. The machine was operating within a 20 cm × 20 cm embroidery frame at a speed of 200 rpm min^{-1}. Film backings (Stocks Embroidery & Sewing Solutions) were attached on the jersey-knitted fabric, which could easily be torn away in water. The conductive yarns severed on the swing bobbin, which were fastened by up and bottom yarns.

Circuitry Assembly: The NTAG NFC chip NT3H2111 (NXP Semiconductor, ISO/IEC 14443, input capacitance of 50 pF) was connected with a microcontroller (TEXAS INSTRUMENTS, MSP430F; voltage range from 1.8 to 3.6 V; operation current of 125 μA), 8 switches and 24 sensors (SILICON LABS, Si7051; voltage range, 1.9–3.6 V; operation current, 195 nA) using the I^{2}C protocol and were assembled into a flexible-PCB.

Strain Test: A tensile testing machine (Instron 3340), an RF Vector Network Analyzer (Keysight AFN9918A-M2) and a StrainMaster (LaVision GmbH 1003017), were connected as a testing system to measure the maximum strain distribution and its corresponding EM properties simultaneously. The tensile load of 100 N was applied at the edges of the coils (vertical direction). The stretching process was captured by a digital camera and analyzed in the StrainMaster system. Images were imported into Photoshop (CC2015, Adobe) to extract the average area changes when coils were deformed.

Measurements of Electromagnetic Properties: An impedance analyzer (Keysight AFN9918A-M2) over a frequency range of 1–20 MHz was used to measure the coil's EM properties (S11, *Q* factor, impedance and operate frequency). Energy-harvesting properties were measured by contacting with a commercial primary coil (TEXAS INSTRUMENTS, TRF7970A) with a spacing of ≈1 mm. The temperature-sensing properties were tested by a programmed APP in the NFC-enabled Android smartphone.

Measurements of Temperature on Newton Thermal Manikin System: The thermal manikin has 35-zone models, and its temperature is controlled

by a thermally conductive carbon-epoxy composite shell with embedded resistance wire heating and sensors. The ambient laboratory temperature was set at 20.75 °C with a relative humidity of 48.8% and wind speed of 0.47 m s^{-1}. We controlled the manikin temperature from 35 to 39 °C and collected the NFC reading data correspondingly.

Supporting Information

Supporting Information is available from the Wiley Online Library or from the author.

Acknowledgements

Conflict of Interest

The authors declare no conflict of interest.

Keywords

[1] A. Scidà, S. Haque, E. Treossi, A. Robinson, S. Smerzi, S. Ravesi, S. Borini, V. Palermo, *Mater. Today* **2018**, *21*, 223.

[2] R. Sun, S. C. Carreira, Y. Chen, C. Xiang, L. Xu, B. Zhang, M. Chen, I. Farrow, F. Scarpa, J. Rossiter, *Adv. Mater. Technol.* **2019**, *4*, 1900100.

[3] J. Jeon, H. B. R. Lee, Z. Bao, *Adv. Mater.* **2013**, *25*, 850.

[4] K. Pan, Y. Fan, T. Leng, J. Li, Z. Xin, J. Zhang, L. Hao, J. Gallop, K. S. Novoselov, Z. Hu, *Nat. Commun.* **2018**, *9*, 5197.

[5] J. Kim, A. Banks, Z. Xie, S. Y. Heo, P. Gutruf, J. W. Lee, S. Xu, K. I. Jang, F. Liu, G. Brown, *Adv. Funct. Mater.* **2015**, *25*, 4761;

[6] J. Kim, A. Banks, H. Cheng, Z. Xie, S. Xu, K. I. Jang, J. W. Lee, Z. Liu, P. Gutruf, X. Huang, *Small* **2015**, *11*, 906.

[7] Y. Moser, M. A. Gijs, *J. Microelectromechan. Syst.* **2007**, *16*, 1349.

[8] W. Zeng, L. Shu, Q. Li, S. Chen, F. Wang, X. M. Tao, *Adv. Mater.* **2014**, *26*, 5310;

[9] J.-S. Roh, Y.-S. Chi, J.-H. Lee, S. Nam, T. J. Kang, *Smart Mater. Struct.* **2010**, *19*, 115020.

[10] L. L. Xu, Y. Li, Y. T. Jang, Z. R. Hu, Y. X. Shi, *Text. Bioeng. Inf. Symp. Proc.* **2017**, *1*, 131.

[11] S. Zhang, A. Chauraya, W. Whittow, R. Seager, T. Acti, T. Dias, Y. Vardaxoglou, *Antennas and Propagation Conf. (LAPC), 2012*, Loughborough, November **2012**.

[12] Z. Wang, L. Zhang, Y. Bayram, J. L. Volakis, *IEEE Trans. Antennas Propag.* **2012**, *60*, 4141.

[13] N. J. Grabham, Y. Li, L. R. Clare, B. H. Stark, S. P. Beeby, *IEEE Sens. J.* **2018**, *18*, 2599.

[14] L. Xu, Y. Liu, Y. Li, P. Y. Lau, H. Si, T. T. Ye, *2018 IEEE Int. Conf. on Service Operations and Logistics, and Informatics (SOLI)*, Singapore, August **2018**.

[15] K. Cherenack, C. Zysset, T. Kinkeldei, N. Münzenrieder, G. Tröster, *Adv. Mater.* **2010**, *22*, 5178.

[16] F. Bardati, S. Iudicello, *IEEE Trans. Biomed. Eng.* **2008**, *55*, 214.

[17] K. Finkenzeller, *RFID Handbook: Fundamentals and Applications in Contactless Smart Cards, Radio Frequency Identification and Near-Field Communication*, John Wiley & Sons, New York **2010**.